Tectonic significance of the Cretaceous granitoids along the southeast coast of continental China

Qiqi Xue [1, 2, *], Yaoling Niu [1, 2, 3, 4, *], Shuo Chen [2, 3, 5], Pu Sun [2, 3], Meng Duan [1, 2], Yajie Gao [2, 3, 5], Di Hong [2, 3, 5], Yuanyuan Xiao [2, 3], Xiaohong Wang [2, 3], Pengyuan Guo [2, 3]

[1] *School of Earth Science and Mineral Resources, China University of Geosciences, Beijing 100083, China*

[2] *Laboratory for Marine Geology, Qingdao National Laboratory for Marine Science and Technology, Qingdao 266061, China*

[3] *Institute of Oceanology, Chinese Academy of Sciences, Qingdao 266071, China*

[4] *Department of Earth Sciences, Durham University, Durham DH1 3LE, UK*

[5] *University of Chinese Academy of Sciences, Beijing 100049, China*

Correspondence

Q. Xue, School of Earth Science and Mineral Resources, China University of Geosciences, Beijing 100083, China.

E-mail: xueq0451@foxmail.com

Y. Niu, Department of Earth Sciences, Durham University, Durham DH1 3LE, UK.

E-mail: yaoling.niu@durham.ac.uk

Highlights

(1) Southeast coastal granitoids of continental China represent the last episode of the magmatism directly associated with the paleo-Pacific plate subduction.

(2) These granitoids resulted from mature crustal melting with significant mantle input.

(3) The along-coast northward $\varepsilon Nd_{(t)}$ and $\varepsilon Hf_{(t)}$ decrease reflects crustal thickening, permitting enhanced crustal assimilation.

Abstract

We present the results of our study on 16 Cretaceous granitoid plutons along the southeast coast of continental China. The zircon U-Pb ages and the bulk-rock Rb-Sr isochron age ($R^2 = 0.935$) indicate that the granitoids represent the last episode of magmatism (119 - 92 Ma) associated with the paleo-Pacific plate subduction beneath continental China. These granitoids show large compositional variation that is to a first-order consistent with varying extents of magma evolution, which is best expressed by a large SiO_2/MgO range and correlated trends of SiO_2/MgO with the abundances and ratios of major and trace elements. The correlated Nd ($\varepsilon Nd_{(t)}$ = -6.1 to -1.2) and Hf ($\varepsilon Hf_{(t)}$ = -4.7 to +3.4) isotopic variation reflects parental magma compositional differences as a result of varying sources and processes. The Nd-Hf isotope data indicate that these granitoids were produced by mature continental crust melting with significant mantle input (~ 20 - 60%). Rhyolite-MELTS modelling shows that relative to the less evolved (i.e., low SiO_2/MgO) granitoid plutons, the progressively more evolved (i.e., varying larger SiO_2/MgO) plutons can be explained by varying extents (~ 25 to 65%) of fractional crystallization. The origin of the magmas parental to the granitoids is best explained by a two-stage process: (1) subducting slab dehydration induced mantle wedge melting for basaltic magmas; and (2) ascent and underplating/intrusion of the basaltic magmas caused the mature crustal melting for the granitoid magmas. The systematic northward decrease in $\varepsilon Nd_{(t)}$ and $\varepsilon Hf_{(t)}$ suggests progressively more enriched crustal material towards the north, but it may very well indicate northward crustal thickening, permitting a greater extent of crustal assimilation.

Key words: Cretaceous granitoids, crust-mantle interaction, crustal thickness variation,

paleo-Pacific plate subduction, southeast continental China

1. Introduction

Mesozoic granitoids are widespread throughout southeast continental China (Figure 1; He, Xu, & Niu, 2010; Zhou et al., 2006), and have been studied for almost a century because of their association with mineralization and their implications on geological evolution of the region (Li et al., 2010; Wu, Li, Yang, & Zheng, 2007). At present, their petrogenesis is generally accepted as being associated with paleo-Pacific plate subduction (Chen, Yang, Zhang, Sun, & Wilde, 2013; Li & Li, 2007; Li, Qiu, & Yang, 2014; Niu et al., 2015; Yang et al., 2018; Zhou & Li, 2000; Zhao, Qiu, Liu, & Wang, 2016), but many important details remain unaddressed. Following the studies of the Jurassic-Cretaceous granitoid widespread in the interiors of the eastern continental China, Niu et al. (2015) argued that all of these granitoids are of intra-plate origin indirectly associated with the paleo-Pacific plate subduction, with a scenario of the paleo-Pacific plate lying horizontally in the mantel transition zone, whose dehydration provided the water that weakened and thinned the mantle lithosphere with the resulting basaltic magmatism responsible for the intra-plate granitoids. However, the granitoids along the southeast coastline are predicted to have directly derived from the overlying crust caused by mantle wedge basaltic magmatism in response to subducting slab dehydration at the time of, or shortly beforehand, the subduction cessation due to the trench jam by an oceanic plateau/microcontinent (the present-day Chinese continental shelf basement) at ~ 100 Ma (Niu et al., 2015).

The significance of this hypothesis is multi-fold, and its testing will offer new perspectives on the petrogenesis of granitoids in general and, more specifically, the Mesozoic geology of the western

Pacific and eastern Eurasia in a global context. A testable aspect of the hypothesis is that the aforementioned "intra-plate" granitoids and the "subducting"-induced coastal granitoids have different sources and magma evolution histories. These differences must be recorded in the petrology and geochemistry of these granitoids. Here, we report new geochemical data on the granitoids from southeast coast of continental China with their age dating results, aiming to 1) explain the petrogenesis of these granitoids; 2) discuss their tectonic implications; and 3) build the basis for comparison with those "intra-plate" granitoids in the interiors of eastern continental China.

2. Geological background and petrography description

2.1 Geological background

The southeast coast of continental China was once located at an active continental margin of the paleo-Pacific plate subduction in the Mesozoic (Figure 1a; Li & Li, 2007; Niu et al., 2015; Zhou et al., 2006). The Zhenghe-Dapu shear zone (ZDSZ) and Changle-Nan'ao shear zone (CNSZ) are two main NE-striking faults in the southeast coastal region of our study (Figure 1b; Shu, Yu, & Wang, 2000; Wang & Shu, 2012; Wang, Sun, Chen, Ling, & Xiang, 2013). Our study is focused on the granitoids along, and in the vicinity of, the CNSZ (Figure 1b).

2.2 Petrography

We collected representative samples from 16 granitoid plutons along the southeast coastline of continental China (Figure 1b). These samples included granodiorite, biotite granite, biotite monzogranite, monzogranite and alkali feldspar granite. The sample and petrographic details are given in Table 1.

The granodiorite consists of quartz, plagioclase, alkali feldspar, amphibole, biotite and accessory minerals (e.g., Fe-Ti oxides, zircon, titanite and apatite; Figures 2a-c). Mafic magmatic enclaves (MMEs) are widespread in the granodiorite and have the same mineralogy as the host. However, the MMEs have greater modal amphibole and biotite than the host (Figure 2a). The biotite granite has varying grain size with a mineral assemblage of quartz, alkali feldspar, plagioclase, biotite and accessory minerals (e.g., Fe-Ti oxides, zircon and apatite; Figure 2d). The biotite monzogranite has a mineral assemblage of quartz, alkali feldspar, plagioclase, biotite and accessory minerals (e.g., Fe-Ti oxides, zircon, apatite and titanite; Figure 2e). They are exposed as a single pluton or composite granitoid complexes. Most of the alkali feldspar granites are equigranular with a graphic texture and mineral assemblage of quartz, alkali feldspar, plagioclase, biotite and accessory minerals (e.g. Fe-Ti oxides, zircon and apatite). Minor arfvedsonite exists in the Kuiqi (FJS14-15) alkali feldspar granite (Figure 2f).

3. Analytical methods

3.1 Zircon U-Pb dating

Zircons were extracted using heavy liquid and magnetic techniques, followed by selection under a binocular microscope. The selected zircons were mounted with epoxy and polished to expose the smooth interiors for cathodoluminescence (CL) imaging and photographing under reflected light. The zircon U-Pb dating was done using the LA-ICP-MS method at the Laboratory of Ocean Lithosphere and Mantle Dynamics (OLMD), Institute of Oceanology, Chinese Academy of Sciences. The instrument consists of an Agilent 7900 inductively coupled plasma mass spectrometry (ICP-MS) coupled with a Photon Machine Excite laser-ablation System. We chose to

106 perform the laser ablation spot analysis on zircons with oscillatory zoning away from inclusions and
107 cracks. We used the single point ablation method with the working parameters of 193 nm wavelength,
108 8 Hz repetition rate, energy of 4.24 J/cm^2 and 35 μm spot size. The data acquisition time for each
109 analysis was 100 s (50 s on background, 50 s on ablated signal). NIST610 was used as the external
110 standard with ^{29}Si as the internal standard. The zircon standard 91500 (Wiedenbeck et al., 1995) was
111 used for quality control (QC) to correct for instrumental drift. The off-line data processing was done
112 using ICPDataCal10.4 (Liu et al., 2010). Isoplot 3.0 (Ludwing, 2003) was used for plotting
113 concordia diagrams and calculating the weighted mean ages.

114 **3.2 Major and trace elements**

115 The whole-rock major element analysis was done using a Leeman Prodigy inductively coupled
116 plasma optical emission spectroscopy (ICP-OES) system at China University of Geosciences in
117 Beijing (CUGB) with precisions better than 1% for most elements except for TiO_2 (~ 1.5%) and
118 P_2O_5 (~ 2.0%) (Song et al., 2010). Loss on ignition (LOI) analysis was measured by placing 0.9 -
119 1.1 g sample in the furnace at 1000 ℃ for 4 - 5 hours before being cooled in a desiccator and
120 reweighted.

121 The whole-rock major element compositions of FJS14-06MME were analyzed at OLMD using
122 an Agilent 5100a ICP-OES instrument. Fifty milligrams of dry rock powder was weighed and fused
123 using 5 times flux sodium metaborate in a platinum crucible. The platinum crucible was placed in
124 the muffle furnace at 1050°C for 60min before being heated on the Bunsen burner. The molten
125 sample was then poured quickly into a beaker with 5% HNO_3. Finally, the sample solution was
126 diluted to ~100 g in a polyethylene bottle for analysis. Precisions for all major elements based on

rock standards STM-2, RGM-2 and W-2 are better than 2%.

Trace element analysis was done using an Agilent 7900 ICP-MS at OLMD. We digested/dissolved 50 mg rock powder with 1 mL Lefort aqua regia solution and 0.5 mL HF in a Teflon beaker and then placed the beaker with the resulting solution with a high-pressure metal "bomb" in an oven at 190°C for 15h. After cooling down, the beaker was kept open on a hotplate at 130°C to incipient dryness before 1 mL HNO_3 was added, and then the mixture was evaporated to incipient dryness. This was followed by adding 1 mL HNO_3 and 4 mL of ultra-pure water in the same beaker to be re-dissolved using the bomb for 2 h. Finally, the sample solution was diluted to 100 g with 2% HNO_3 in a polyethylene bottle for analysis (Chen et al., 2017). The analytical precision was better than 5%, and the accuracy was generally better than 10% for all elements but Be (12%).

3.3 Mineral compositions

We chose plagioclase with concentric zoning for major element analysis in the laboratory of Langfang Institute of Regional Geological Survey using a JEOL EPMA-8230 electron-microprobe (EMP) with a beam size of 5 μm diameter, at 15 kV and 20 μA beam current.

3.4 Whole-rock Sr-Nd-Hf isotopes

The whole-rock Sr-Nd-Hf isotopic compositions were analyzed using a Nu Plasma HR multi-collector inductively coupled plasma mass spectrometry (MC-ICP-MS) system in the Radiogenic Isotope Facility at the University of Queensland (RIF-UQ), Australia with sample preparation and analytical details given in Guo et al. (2014). The measured $^{87}Sr/^{86}Sr$, $^{143}Nd/^{144}Nd$ and $^{176}Hf/^{177}Hf$

147 ratios were corrected for mass fractionation using the exponential law by normalizing to $^{86}Sr/^{88}Sr$ =
148 0.1194, $^{146}Nd/^{144}Nd$ = 0.7219 and $^{179}Hf/^{177}Hf$ = 0.7325, respectively. The measured average value
149 for the NBS-987 Sr standard was $^{87}Sr/^{86}Sr$ = 0.710249±17 (n = 23, 2σ). The Nd metal 50ppb, an in-
150 house Nd standard, had an average $^{143}Nd/^{144}Nd$ of 0.511966±6 (n = 21, 2σ). The repeated
151 measurement of the Hf standard (40 ppb) gave an average $^{176}Hf/^{177}Hf$ value of 0.282145±6 (n = 14,
152 2σ). The Geological Survey of Japan (GSJ) rock reference sample JG-3 and the U.S. Geological
153 Survey (USGS) rock standard BCR-2 were repeatedly measured along with our samples. Repeated
154 analysis of JG-3 along with our samples gave $^{87}Sr/^{86}Sr$ = 0.705379±16 (n = 2, 2σ), $^{143}Nd/^{144}Nd$ =
155 0.512612±7 (n = 2, 2σ) and $^{176}Hf/^{177}Hf$ = 0.282883±5 (n = 2, 2σ). Repeated analysis of BCR-2 run
156 along with our samples gave $^{87}Sr/^{86}Sr$ = 0.705022±13 (n = 2, 2σ), $^{143}Nd/^{144}Nd$ = 0.512627±6 (n =
157 2, 2σ) and $^{176}Hf/^{177}Hf$ = 0.282866±6 (n = 2, 2σ). The JG-3 and BCR-2 run with our samples gave
158 values consistent with the reference values (GeoReM, http://georem.mpch-mainz.gwdg.de/;
159 González- Guzmán, Weber, Manjarrez, Hecht, & Solari, 2014; Takashi & Kenji, 1998).

160 **4. Results**

161 **4.1 Zircon U-Pb ages**

162 Zircon U-Pb age data for the Zhao'an (FJS14-01), Xiamen (FJS14-08) and Putian (FJS14-13)
163 plutons are given in Appendix 1 and presented in Figures 3a-f. All zircons are colourless, transparent
164 and columnar grains. The CL images show that they are mostly euhedral and 70 - 200 μm long with
165 length/width ratio of 1:1 - 4:1. They have the characteristics of magmatic zircons with oscillatory
166 zoning (Figures 3a-c). Zircons from the Zhaoan pluton (FJS14-01) have varying Th and U with a
167 Th/U ratio of 0.19 - 1.01 (Appendix 1), and give a weighted mean $^{206}Pb/^{238}U$ age of 101.3 ± 2.8 Ma

(n = 11, MSWD = 3.5) (Figure 3d), representing the crystallization age of the Zhaoan pluton. Zircons from the Xiamen pluton (FJS14-08) have relatively high Th and U with a Th/U ratio of 0.54 - 0.79 (Appendix 1), and give a weighted mean $^{206}Pb/^{238}U$ age of 117.6 ± 1.6 Ma (n = 6; MSWD = 0.97) (Figure 3e) after rejecting the discordant data. This age is similar to the age of 114.8 ± 1.8 Ma in the literature (Yang et al., 2018). Zircons from the Putian pluton (FJS14-13) also have varying Th and U, with a Th/U ratio of 0.69 - 2.63 (Appendix 1), and give a weighted mean $^{206}Pb/^{238}U$ age of 109.0 ± 1.1 Ma (n = 11, MSWD = 1.09) (Figure 3f).

Our zircon U-Pb ages and the zircon U-Pb ages from the literature (Appendix 2), indicate that the magmatism occurred at 119 - 118 Ma (2 samples), 111 - 108 Ma (3 samples) and 103 - 92 Ma (11 samples). In fact, these zircon U-Pb ages on the selected samples are consistent with the whole-rock Rb/Sr isochron age of 100±2 Ma, representing the mean emplacement age of these granitoid plutons (see Figure 7g below).

4.2 Major and trace elements

Whole-rock major and trace element data are given in Appendices 3 and 4. The granitoids show a large compositional variation that is to a first-order consistent with varying extents of magma evolution as shown by a large SiO_2/MgO range (17 - 2082) (Figure 4). With the increase of SiO_2/MgO ratio, the granitoids are progressively more evolved and can be divided into three groups for the convenience of discussion (Figure 4). This grouping also applies to the abundances and ratios of incompatible trace elements (Figure 5; Appendix 4 and Appendix 8).

Group 1 samples (from Gunong, Changtai and Danyang plutons with the lowest SiO_2/MgO of 17 - 45) are mainly granodiorites, dated from 100 to 97 Ma. They have the highest TiO_2, Al_2O_3,

189 $^{T}Fe_2O_3$, CaO, P_2O_5 and A/NK (Figure 4; Appendix 3 and Appendix 7). These granitoids are enriched
190 in large ion lithosphere elements (LILEs, e.g. Rb, Th, U and Pb) and depleted in high field strength
191 elements (HFSEs, e.g. Nb, Ta, Ti and Zr) and show weak negative Ba and Sr anomalies and varying
192 $(La/Yb)_N$ of 7.39 - 22.71 (Appendix 4). The LREE fractionation is pronounced with high $(La/Sm)_N$
193 of 3.31 - 5.67, whereas the HREEs are relatively flat with $(Gd/Yb)_N$ = 1.51 - 2.23 (Appendix 4).
194 Group 1 samples have weak negative Eu anomalies (Figure 5b; Appendix 4; Eu/Eu^* = 0.39-0.76;
195 $Eu/Eu^* = 2Eu_N/(Sm_N + Gd_N)$; where the subscript N refers to chondrite-normalized value). Both the
196 host and MME show a similar magnitude of negative Eu anomalies.
197 Group 2 samples (from Zhao'an, Huxi, Changqiao, Xiamen, Huacuo, Weitou, Quanzhou,
198 Putian, Dacenshan and Nanzhen plutons with a high SiO_2/MgO of 166 - 1128) are biotite granite,
199 biotite monzogranite and monzogranite, dated from 119 to 93 Ma. They have lower TiO_2, Al_2O_3,
200 $^{T}Fe_2O_3$, CaO, P_2O_5 and A/NK than Group 1 (Figure 4; Appendix 3). These granitoids are more
201 enriched in LILEs (e.g. Rb, Th, U and Pb), depleted in HFSEs (e.g. Nb, Ta, Ti and Zr), and show
202 moderate Ba and negative Sr anomalies with varying $(La/Yb)_N$ ratios of 5.49 - 15.72 (Appendix 4).
203 The LREE fractionation is pronounced with $(La/Sm)_N$ = 3.43 - 7.33, whereas the HREEs are
204 relatively flat with $(Gd/Yb)_N$ = 0.93-2.43. They have negative Eu anomalies (Figure 5b; Appendix
205 4; Eu/Eu^*=0.31-0.87).
206 Group 3 samples (from Chengxi, Kuiqi and Sansha plutons with SiO_2/MgO of 1345 - 2082)
207 are highly evolved alkali feldspar granites, dated from 101 - 92 Ma. They thus have extremely high
208 SiO_2/MgO and low CaO with similar levels of TiO_2, Al_2O_3 and $^{T}Fe_2O_3$ to Group 2 samples (Figure
209 4; Appendix 3). Their extreme enrichment in LILEs (e.g. Rb, Th, U and Pb), depletion in HFSEs
210 (e.g. Nb, Ta, Ti and Zr) and strong negative Ba and Sr anomalies (Appendix 4; Eu/Eu^*=0.06 - 0.19)

211 are expected as the result of advanced extents of fractionation, which is also consistent with the
212 varying $(La/Yb)_N$ (2.84 - 7.10), $(La/Sm)_N$ (2.91 - 6.61), and $(Gd/Yb)_N$ (1.04 - 1.47) ratios (Appendix
213 4).

214 Therefore, with increasing SiO_2/MgO, samples from Group 1 to Group 3 are progressively
215 more evolved with decreasing TiO_2, Al_2O_3, $^TFe_2O_3$, CaO, P_2O_5, A/NK ratio (Figure 4), Ba and
216 Eu/Eu* ratio (Figure 5b) and increasing Nb and Rb/Sr ratio (Figures 5c-d). The tree groups are all
217 relatively depleted in HFSEs with overlapping REE ratios (Appendix Figure). They have a similar
218 A/CNK ratio but varying A/NK values with Group 1 > Group 2 > Group 3, which is consistent with
219 the progressive removal of Al_2O_3 and CaO because of Ca-rich plagioclase fractionation (Figure 4).

220 **4.3 Plagioclase compositions**

221 The data are given in Appendix 5. Plagioclase from two granodiorite host-MME pairs (FJS14-
222 06host - MME; FJS14-17host - MME) was analyzed to understand the significance of the MMEs in
223 the context of the granitoid petrogenesis. Plagioclase in the MME from the Changtai pluton (FJS14-
224 06) has An_{40-55} (Figure 6a), which is much higher than that in the granodiorite host with An_{25-39}
225 (Figure 6b). Plagioclase in the MME from the Danyang pluton (FJS14-17; Figure 6c; An=33-47) is
226 similar to or more calcic than that in the granodiorite host (Figure 6d; An = 23 - 41).

227 **4.4 Whole-rock Sr-Nd-Hf isotopes**

228 Whole-rock Sr-Nd-Hf isotopic compositions are given in Appendix 6. The correlated Nd ($\varepsilon Nd_{(t)}$
229 = -6.09 to -1.158) and Hf ($\varepsilon Hf_{(t)}$ = -4.68 to +3.35) isotopic variation reflects parental magma
230 compositional differences as the result of varying sources and processes of the granitoids. The

observed large Sr isotopic variation ($^{87}Sr/^{86}Sr$ = 0.7068 to 1.311) is consistent with the large Rb/Sr ratio variation among samples (Figure 5d; Shao, Niu, Regelous, & Zhu, 2015; Wu et al., 2007) and gives a significant (>99% confidence level) isochron age of 100±2 Ma (Figure 7g), representing the mean emplacement age of the granitoids.

5. Discussion

5.1 Temporal-spatial distribution

Zhou and Li (2000) reported that the granitoids are progressively younger from the interior toward the southeast coast of continental China. However, Li and Li (2007) argued that the temporal-spatial distribution of the magmatism is more complex. Sun (2006) and Zhou et al. (2006) showed that the Cretaceous granites are distributed in a very large area of the Cathaysia block, which is ~1000 km long and 500 km wide, rather than liner distribution along the coastline. More recently, Niu et al. (2015) demonstrated that in eastern continental China, the Jurassic-Cretaceous (~190 - ~90 Ma) granitoids are distributed randomly in space and time in a wide zone in excess of >1000 km. Such granitoid distributions in space and time are best explained as a special consequence of plate tectonics, genetically associated with the paleo-Pacific plate subduction beneath eastern continental China (Niu, 2005; 2014). Specifically, the dehydration of the paleo-Pacific plate stagnant horizontally in the mantle transition zone beneath eastern continental China ultimately caused the lithosphere thinning and basaltic magmatism. Underplating and intrusion of such basaltic magmas indirectly caused the crustal melting and the widespread granitoid magmatism in the interiors of eastern continental China (i.e., “intra-plate” granitoid magmatism; Niu et al., 2015).

The youngest granitoids along the coastal region of southeast continental China of ~ 90Ma

indicate the cessation of the paleo-Pacific plate subduction at this time or slightly earlier at ~ 100 Ma, caused by the trench jam upon the arrival of a microcontinent (the present-day Chinese continental shelf basement; Niu et al., 2015). This means that the coastal granitoids represent the last episode of the granitoid magmatism in response to the paleo-Pacific plate subduction in the Cretaceous (Niu et al., 2015). This understanding leads to the hypothesis that the coastal granitoids are immediately "subduction" related and differ from those "intra-plate" granitoids in the interiors of eastern continental China. Indeed, the coastal granitoids we report here have significantly greater mantle input than the "intra-plate" granitoids (our unpublished data).

5.2 Petrogenesis

5.2.1 Host and MMEs

Samples FJS14-06host and FJS14-06MME of the Changtai pluton have similar $^{87}Sr/^{86}Sr_{(i)}$ (0.705961; 0.705928), $\varepsilon Nd_{(t)}$ (-3.24; -3.29) and $\varepsilon Hf_{(t)}$ (-0.92; -0.55) isotopic ratios (Appendix 6; Figures 7a-d), indicating that they share the same parental magma (Chen et al., 2016; 2018). Their small differences in major and trace element abundances are controlled by the model mineralogy with the MMEs having greater modal amphiboles crystallized at early stage of the same system. This is also consistent with the MMEs having higher plagioclase An than that of the host (Appendix 5).

5.2.2 Genetic relationship between the coastal granitoids

Although previous studies agreed that the petrogenesis of the coastal granitoids involved significant crustal material (Chen & Jahn, 1998; Jahn et al., 1990), different views exist, including

that 1) the granitoids were formed by different degrees of fractional crystallization of magmas produced by crust-mantle interaction (Qiu et al., 2004; 2008); 2) these granitoids were crystallized from magmas formed by the partial melting of prior tonalitic to granodioritic rocks (Zhao et al., 2015); and 3) mantle-derived mafic magmas mixed with crust-derived magmas (Zhao et al., 2016). However, most of these previous studies focused on single plutons or composite granitoid complexes without along-coast regional comparison.

The overlapping zircon U-Pb ages (Figure 3) and Nd and Hf isotopic compositions (Figure 7) suggest that the 3 Group granites must have been produced in the same timeframe and share similar sources and processes in term of their parental magma generation. The high SiO_2/MgO (Figures 4, 5), high Rb/Sr (Figure 5d) and low Ba and Eu/Eu* of the Group 3 samples are consistent with their being highly evolved products of a similar magmatic lineage (Figures 4, 5).

The correlated Nd ($\varepsilon Nd_{(t)}$ = -6.1 to -1.2) and Hf ($\varepsilon Hf_{(t)}$ = -4.7 to +3.4) isotopic variations (Figure 7b) between samples reflect their parental magma compositional differences inherited from varying sources and processes. Figures 7c-d show that there is mantle contribution to the granitoids, a scenario that has long been recognized (Deng et al., 2016; Li et al., 2014; Li & Li., 2007; Li, Qiu, & Xu, 2012; Zhou & Li., 2000). The best interpretation is that these granitoids result from melting of mature crustal material (lower Nd-Hf isotopes) triggered by mantle-derived melts (higher Nd-Hf isotopes) that contributed both heat and materials. Furthermore, a simple mixing calculation suggests ~20-60% mantle contribution to the petrogenesis of these granitoids in terms of Nd-Hf isotopes (Figure 7b; Appendix 6).

5.2.3 The cause of the large SiO_2/MgO range

We stated above that the large SiO_2/MgO range of these granitoid plutons represented by our samples resulted from varying extent of fractional crystallization from their respective parental magmas (Figures 4, 5). To quantify this interpretation, we applied the Rhyolite-MELTS (Gualda et al., 2012) to model the crystallization processes. We used the composition of the Group 1 sample (FJS14-06host) with the lowest SiO_2/MgO and 6 wt. % H_2O to approximate the primitive parental magmas. The calculation was done at 3 kbars. The mineralogy chosen in the calculation was based on the petrography. The results explain the data as expected in terms of the SiO_2/MgO ratio (Figures 4, 5). Relative to the Group 1 sample (FJS14-06host), the extents of fractional crystallization of the Group 2 and Group 3 samples were ~24-51% and ~51-64%, respectively (Figure 9a). In Figure 9b, all samples display progressive fractional crystallization dominated by plagioclase and K-feldspar with the Group 3 samples having the highest extent of fractional crystallization (Figure 4 & Figure 9a).

In summary, the parental magmas of these granitoids were derived from crustal melting induced by mantle-derived melts equivalent to ~20-60% mantle contribution in terms of Nd-Hf isotopes (Figure 7b). The varying extent of fractional crystallization of such parental magmas, as manifested by the varying SiO_2/MgO ratios of the 3 groups of granitoid samples (Figures 4, 5, 9), formed these coastal granitoids.

5.2.4 The classification of the granitoids

This is not the focus of the paper, but the discussion is necessary here. In studying the petrogenesis of granites and granitoids, it is common that researchers classify the rocks into M-type, I-type, S-type and A-type granite/granitoids (Chappell & White., 1992; Pitcher., 1983; Whalen,

314 Currie, & Chappell, 1987). Such classification has also been emphasized in studying the Cretaceous
315 granitoids along the southeast coast of continental China in the past 20 years (Li et al., 2007; Li,
316 Qiu, Jiang, Xu, & Hu, 2009; Liu et al., 2012; Qiu et al., 2008; Wu et al., 2003; Xiao et al., 2007).
317 However, we show that such classification or "discrimination" diagrams have no significance at
318 least for the granitoids that we studied along the southeast cost of continental China. This is because
319 the tectonic setting of these granitoids is known and tectonically well-constrained (see above and
320 below), but if we were indiscriminately applying such classification, we would be both misled and
321 misleading in terms of tectonic settings. For example, it is clear from the SiO_2/MgO variation
322 diagrams (Figures 4, 5) that our granitoid samples represent varying degrees of magma evolution
323 (dominantly fractional crystallization) from spatially and temporally similar parental magmas,
324 rather than genetically different S-, I-, and A-types or fractionated (FG) or unfractionated (OGT)
325 types of granitoids as shown in Figure 8.

326 **5.3 Geological background**

327 Zhou and Li (2000) proposed that the subducting slab of the paleo-Pacific plate steepened (slab
328 rollback) during 180-80 Ma and varying degrees of mantle wedge melting produced basaltic
329 magmas. These basaltic magmas rose and heated the lower continental crust to produce the felsic
330 magmas parental to the granitoids in the region. Li and Li (2007) proposed a flat-slab subduction
331 model to explain the formation of the ~1300 km wide intracontinental orogen during 265 - 190 Ma
332 and used the flat-slab break off model to explain the 190 - 80 Ma south China granitoid petrogenesis.
333 The appearance of the A-type granite (190 Ma) in southern Jiangxi province would suggest a
334 tectonic setting change. Li and Li (2007) suggested that the trend of granitoids becoming younger

toward the coast after 150 Ma was caused by the breakup of the flat subducting slab. Niu (2005; 2014) and Niu et al. (2015) suggested that the Mesozoic granitoids throughout eastern continental China have connection with the lithospheric thinning in eastern China and resulted from "basal hydration weakening" caused by dehydration of the subducted slab lying in the mantle transition zone.

Compared with the coeval granitoids in the vast interiors of eastern continental China, or the "intra-plate" granitoids, which are genetically and ultimately associated with the mantle transition-zone paleo-Pacific slab dehydration, lithosphere thinning and basaltic magmatism (Niu, 2014; Niu et al., 2015), the granitoids we studied along the southeast coastline of continental China are directly caused by paleo-Pacific plate subduction although the detailed history of such subduction remains controversial (Deng et al., 2016; Li, 2000; Li & Li, 2007; Li, Zhou, Chen, Wang, & Xiao, 2011; Li et al., 2012; Li et al., 2014; Lin, Cheng, Zhang, & Wang, 2011; Mao, Li, & Wang, 1998; Niu., 2014; Shan et al., 2014; Wu, Dong, Wu, Zhang, & Ernst, 2017; Zhao, Hu, Zhou, & Liu, 2007; Zhao et al., 2015). With all the observations and above discussions considered, we propose that the granitoids in the present study represent the last episode of magmatism associated with the paleo-Pacific plate subduction beneath continental China at the time of, or shortly before, the trench jam and cessation of the subduction, whose locus is marked by the arc-shaped southeast coastline of continental China (Niu et al., 2015). This scenario can be readily explained by the subducting slab dehydration induced mantle wedge melting and basaltic magma generation (Figure 10a). The basaltic magmas produced in this way ascend and underplate/intrusion the mature crust, contributing both heat and material for crustal melting and granitoid magma generation, which is also consistent with both mantle and crustal contributions indicated by the Nd-Hf isotopes (Figure 7). These results confirm previous

interpretation (Chen et al., 2013; Qiu et al., 2008; Qiu et al., 2012) and offer a general solution to the petrogenesis of all the Cretaceous granitoids along the southeast coast of the continental China.

An important new observation is that the granitoids show a northward $\varepsilon Nd_{(t)}$ and $\varepsilon Hf_{(t)}$ (Figures 7e, f) isotopic decrease, which may be caused by several possibilities, including, as one travels northward (1) there are more terrigenous sediments contributed to the mantle wedge for the basaltic magmatism in the first place, (2) there are compositional differences of the existing crust, and (3) there is increasing crustal thickness for higher extent of crustal assimilation. With all factors considered, the best interpretation is the northward crustal thickening, permitting a greater extent of crustal assimilation (Figure 10b).

6. Conclusions

(1) We report for the first time the zircon U-Pb ages for the Zhaoan (101±3 Ma) and Putian (109±1 Ma) plutons (Figure 3). The zircon U-Pb age of the Xiamen pluton (118±2 Ma) agrees with the age data in the literature. These age data on selected granitoid samples and the whole-rock Rb-Sr isochron age of 100±2 Ma (Figure 7) on all of the studied plutons together place constraints on the coastal granitoids representing the last episode of the magmatism associated with the paleo-Pacific plate subduction, with the magmatism ending because of the subduction cessation at ~ 100 Ma.

(2) The origin of the magmas parental to these granitoids is best understood as resulting from paleo-Pacific slab subducting induced mantle wedge melting, whose basaltic melt intruded/underplated the crust for the crustal melting and granitoid production (Figure 10). This is manifested by both mantle (20-60%) and crustal (40-80%) contributions to the

granitoids in terms of Nd-Hf isotope compositions (Figure 7b).

(3) A varying extent of fractional crystallization dominated magma evolution resulted in the observed compositional diversity of these granitoids as expressed in the SiO_2/MgO variation diagrams (Figures 4, 5). Rhyolite-MELTS modelling suggests that relative to Group 1 samples (FJS14-06host), the extent of fractional crystallization of Group 2 and Group 3 samples was ~24 - 51% and ~51 - 64%, respectively (Figure 9a). Group 2 samples displayed a progressive fractional crystallization of plagioclase and orthoclase, and Group 3 samples showed further fractional crystallization dominated by orthoclase.

(4) The northward $\varepsilon Nd_{(t)}$ and $\varepsilon Hf_{(t)}$ increase is best explained as northward crustal thickening (Figures 7e-f), which permits enhanced crustal magma assimilation.

(5) The widely used classification or finger-printing geochemical diagrams for granitoids (Figure 8) have no significance, at least for the granitoids that we studied.

Acknowledgments

We thank Li Jiyong, Shao Fengli and Ye Lei for fieldwork assistance, Qin Hong and Su Li for assistance in major and trace element analysis. This work was supported by the National Natural Science Foundation of China (NSFC41630968, 41130314, 41776067), the Chinese Academy of Sciences (Innovation Grant Y42217101L), the Scientific and Technological Innovation Project Financially Supported by Qingdao National Laboratory for Marine Science and Technology (No.2015ASKJ03), the NSFC-Shandong Joint Fund for Marine Science Research Centers (U1606401) and 111 Project (B18048).

References

399 Chappell, B.W., White, A.J.R. (1992). I- and S-type granites in the Lachlan Fold Belt. Geological
400 Society of America Special Papers, 272, 1-26.
401 Chen, C. H., Lu, H.Y., Lin, W., Lee, C.Y. (2006). Thermal event records in SE China coastal areas:
402 Constraints from Monazite Ages of Beach Sands from two sides of the Taiwan Strait. Chemical
403 Geology, 231, 118-134.
404 Chen, J.Y., Yang, J.H., Zhang, J.H., Sun, J.F., Wilde, S.A. (2013). Petrogenesis of the Cretaceous
405 Zhangzhou batholith in southeastern China: zircon U-Pb age and Sr-Nd-Hf-O isotopic evidence.
406 Lithos, 162-163, 140-156.
407 Chen, S., Niu, Y.L., Li, J.Y., Sun, W.L., Zhang, Y., Hu, Y., Shao, F.L., 2016. Syncollisional adakitic
408 granodiorites formed by fractional crystallization: insights from their enclosed mafic magmatiuc
409 enclaves (MMEs) in the Qumushan pluton, North Qilian Orogen at the northern margin of the
410 Tibetan Plateau. Lithos, 248/251, 455-468.
411 Chen, S., Wang, X.H., Niu, Y.L., Sun, P., Duan, M., Xiao, Y.Y., ..., Xue, Q.Q. (2017). Simple and
412 cost-effective methods for precise analysis of trace element abundances in geological materials
413 with ICP-MS. Science Bulletin, 62, 277-289.
414 Deng, J.F., Feng, Y.F., Di, Y.J., Liu, C., Xiao, Q.H., Su, S.G., ..., Xiong, L. (2016). The Intrusive
415 Spatial Temporal Evolutional Framework in the Southeast China. Geological Review, 62, 3-16
416 (in Chinese with English abstract).
417 González-Guzmán, R., Weber, B., Manjarrez-Juárez, R., Hecht, L., Solari, L. (2014). Petrogenesis
418 of basement rocks in the southern Chiapas Massif: Implications on the tectonic evolution of the
419 Maya Block. Goldschmidt.
420 Gualda, G.A.R., Ghiorso, M.S., Lemons, R.V., Carley, T.L. (2012). Rhyolite-MELTS: a modified

421 calibration of MELTS optimized for silica-rich, fluidbearing magmatic systems. Journal of
422 Petrology, 53, 875-890.
423 Guo, P.Y., Niu, Y.L., Ye, L. Liu, J.J., Sun, P., Cui, H.X., ..., Feng, Y.X. (2014). Lithosphere thinning
424 beneath west North China Craton: Evidence from geochemical and Sr-Nd-Hf isotope
425 compositions of Jining basalts. Lithos, 202/203, 37-54.
426 He, Z.Y., Xu, X.S., Niu, Y.L. (2010). Petrogenesis and tectonic significance of a Mesozoic granite-
427 syenite-gabbro association from inland South China, Lithos, 119, 621-641.
428 Li, L.L., Zhou, H.W., Chen, Z.H., Wang, J.R., Xiao, Y. (2011). Geochemical characteristics of
429 granites in Taimushan area, Fujian Province, and their geological significance. Acta Petrologica
430 Et Mineralogica, 30, 593-609.
431 Li, X.H. (2000). Cretaceous magmatism and lithosphere extension in Southeast China. Journal of
432 Asian Earth Sciences 18, 293-305.
433 Li, X.H., Li, W.X., Wang, X.C., Li, Q.L., Liu, Y., Tang, G.Q., Gao, Y.Y., Wu, F.Y. (2010). SIMS
434 U-Pb zircon geochronology of porphyry Cu-Au-(Mo) deposits in the Yangtze River
435 Metallogenic Belt, eastern China: magmatic response to Early Cretaceous lithospheric extension.
436 Lithos, 119, 427-438.
437 Li, X.H., Li, Z.X., Li,W.X., Liu, Y., Yuan, C.,Wei, G.J., Qi, C.S. (2007). U-Pb zircon, geochemical
438 and Sr-Nd-Hf isotopic constraints on age and origin of Jurassic I- and A-type granites from
439 central Guangdong, SE China: a major igneous event in response to foundering of a subducted
440 flat-slab? Lithos, 96, 186-204.
441 Li, Z., Qiu, J.S., Jiang, S.Y., Xu, X.S., Hu, J. (2009). Petrogenesis of the Jinshan Granitic Composite
442 Pluton in Fujian Province: Constraints from Elemental and Isotopic Geochemistry. Acta

443 Geologica Sinica, 83, 515-527.
444 Li, Z., Qiu, J.S., Xu, X.S. (2012). Geochronological, geochemical and Sr-Nd-Hf isotopic constraints
445 on petrogenesis of late Mesozoic gabbro-granite complexes in the southeast coast of Fujian,
446 South China: insights into a depleted mantle source region and crust-mantle interactions.
447 Geological Magazine, 149, 459-482.
448 Li, Z., Qiu, J.S., Yang, X.M. (2014). A review of the geochronology and geochemistry of Late
449 Yanshanian (Cretaceous) plutons along the Fujian coastal area of southeastern China:
450 Implications for magma evolution related to slab break-off and rollback in the Cretaceous. Earth
451 Science Reviews, 128, 232-248.
452 Li, Z.X., Li, X.H. (2007). Formation of the 1300-km-wide intracontinental orogen and postorogenic
453 magmatic province in Mesozoic South China: a flat-slab subduction model. Geology, 35, 179-
454 182.
455 Lin, Q.C., Cheng, X.W., Zhang, Y.Q., Wang, F.Y. (2011). Evolution of granitoids in the active
456 continental margin: a case study of the Fuzhou Compound Complex. Acta Geologica Sinica, 85,
457 1128-1133 (in Chinese, with English abstract).
458 Liu, Q., Yu, J.H., Wang, Q., Su, B., Zhou, M.F., Xu, H., Cui, X. (2012). Ages and geochemistry of
459 granites in the Pingtan-Dongshan Metamorphic Belt, Coastal South China: new constraints on
460 Late Mesozoic magmatic evolution. Lithos, 150, 268-286.
461 Liu, Y. S., Gao, S., Gao, C.G., Hu, Z.C., Wang, D.B., Zong, K.Q. (2010). Continental and oceanic
462 crust recycling-induced melt-peridotite interactions in the Trans-North China Orogen: U-Pb
463 dating, Hf isotopes and trace elements in zircons from mantle xenoliths. Journal of Petrology,
464 51, 537-571.

Ludwig, K.R. (2003). User's manual for Isoplot 3.00: A geochronological toolkit for Microsoft Excel, Special Publication 4: Berkeley, CA., Berkeley Geochronology Center, 1-70.

Mao, J.W., Li, H.Y., Wang, D.H. (1998). Ore-froming of Mesozoic polymetallic deposits in South China and its relationship with mantle plume. Bulletin of Mineralogy, Petrology and Geochemistry, 19, 130-132.

Miyazaki, T. (2008). Sr and nd isotope ratios of twelve gsj rock reference samples. Geochemical Journal, 32, 345-350.

Niu, Y.L. (2005). Generation and evolution of basaltic magmas: Some basic concepts and a hypothesis for the origin of the Mesozoic-Cenozoic volcanism in eastern China. Geological Journal of China Universities 11, 9-46.

Niu, Y.L. (2014). Geological understanding of plate tectonics: Basic concepts, illustrations, examples and new perspectives. Global Tectonics and Metallogeny 10, 23-46.

Niu, Y.L., Liu, Y., Xue, Q.Q., Shao, F.L., Chen, S., Duan, M., ..., Zhang, Y. (2015). Exotic origin of the Chinese continental shelf: new insights into the tectonic evolution of the western Pacific and eastern China since the Mesozoic. Science Bulletin, 60, 1598-1616.

Pitcher, W.S. (1983). Granite type and tectonic environment. In: Hsu, K. (ed) Mountain Buiding Processes. Academic Press, London, 19-40.

Qiu, J.S., Li, Z., Liu, L., Zhao, J.L. (2012). Petrogenesis of the Zhangpu composite granite pluton in Fujian province: constraints from zircon U–Pb ages, elemental geochemistry and Nd–Hf isotopes. Acta Geologica Sinica, 86, 561–576 (in Chinese with English abstract).

Qiu, J.S., Wang, D.Z., Mcinnes, B.I.A., Jian, S.Y., Wang, R.C., Kanisawa, S. (2004). Two subgroups of A-type granites in the coastal area of Zhejiang and Fujian Provinces, SE China:

487 age and geochemical constraints on their petrogenesis. Transactions of the Royal Society of
488 Edinburgh: Earth Sciences, 95, 227-36.
489 Qiu, J.S., Xiao, E., Hu, J., Xu, X.S., Jiang, S.Y., Li, Z. (2008). Petrogenesis of highly fractionated
490 Itype granites in the coastal area of northeastern Fujian Province: constraints from zircon U-Pb
491 geochronology, geochemistry and Nd-Hf isotopes. Acta Petrolei Sinica, 24, 2468-2484 (in
492 Chinese with English abstract).
493 Rudnick, R., Gao, S. (2003). Composition of the continental crust. Treatise on Geochemistry, 3, 1-
494 64.
495 Salters, V.J.M., Stracke, A. (2004). Composition of the depleted mantle. Geochemistry Geophysics
496 Geosystems 5, 1525-2027.
497 Shan, Q., Zeng, Q.S., Li, J.K., Lu, H.Z., Hou, M.Z., Yu, X.Y., Wu, C.J. (2014). U-Pb geochronology
498 of zircon and geochemistry of Kuiqi miarolitic granites, Fujian Province. Acta Petrologica Sinica,
499 30, 1155-1167 (in Chinese with English abstract).
500 Shao, F.L., Niu, Y.L., Regelous, R., Zhu, D.C. (2015). Petrogenesis of peralkaline rhyolites in an
501 intra-plate setting: Glass House Mountains, Southeast Queensland, Australia. Lithos, 216/217,
502 196-210.
503 Shen, W.Z., Zhu, J.C., Liu, C.S., Xu, S.J., Ling, H.F. (1993). Sm-Nd isotopic study of basement
504 metamorphic rocks in south China and its constraint on material sources of granitoids. Acta
505 Petrologica Sinica, 9, 115-124 (in Chinese, with English abstract).
506 Shu, L.S., Yu, J.H., Wang, D.Z. (2000). Late Mesozoic granitic magmatism and metamorphism-
507 ductile deformation in the ChangleeNanao fault zone, Fujian Province. Geological Journal of
508 China Universities, 6, 368-378.

509 Song, S., Su, L., Li, X.H., Zhang, G., Niu, Y., Zhang, L. (2010). Tracing the 850-Ma continental
510 flood basalts froma piece of subducted continental crust in the North Qaidam UHPM belt, NW
511 China. Precambrian Research, 183, 805-816.
512 Sun, T. (2006). A new map showing the distribution of granites in South China and its explanatory
513 notes. Geological Bulletion of China, 25, 332-335 (in Chinese, with English abstract).
514 Takashi, M., Kenji, S. (1998). Sr and Nd isotope ratios of twelve GSJ rock reference samples.
515 Geochemical Journal, 32, 345-350.
516 Wang, D.Z., Shu, L.S. (2012). Late Mesozoic basin and range tectonics and related magmatism in
517 Southeast China. Geoscience Frontiers, 3, 109-124.
518 Wang, K.X., Sun, T., Chen, P.R., Ling, H.F., Xiang, T.F. (2013). The geochronological and
519 geochemical constraints on the petrogenesis of the Early Mesozoic A-type granite and diabase
520 in northwestern Fujian province. Lithos, 179, 364-381.
521 Whalen, J.B., Currie, K.L., Chappell, B.W. (1987). A-type granites: geochemical characteristics,
522 discrimination and petrogenesis. Contributions to Mineralogy and Petrology, 95, 407-419.
523 Wiedenbeck, M.A.P.C., Alle, P., Corfu, F., Griffin, W.L., Meier, M., Oberli, F.V., ..., Spiegel, W.
524 (1995). Three natural zircon standards for U-Th-Pb, Lu-Hf, trace element and REE analyses.
525 Geostandards and Geoanalytical Research, 19, 1-23.
526 Wu, C.L., Dong, S.W., Wu, D., Zhang, X., Ernst, W. G. (2017). Late Mesozoic high-K calc-alkaline
527 magmatism in Southeast China: the Tongling example. International Geology Review, 1-35.
528 Wu, F.Y., Jahn, B.M., Wilde, S.A., Lo, C.H., Yui, T.F., Lin, Q., Ge, W.C., Sun, D.Y. (2003). Highly
529 fractionated I-type granites in NE China (II): isotopic geochemistry and implications for crustal
530 growth in the Phanerozoic. Lithos, 67, 191-204.

Wu, F.Y., Li, X.H., Yang, J.H., Zheng, Y.F. (2007). Discussions on the petrogenesis of granites. Acta Petrologica Sinica, 23, 1217-1238 (in Chinese with English abstract).

Xiao, E., Qiu, J.S., Xu, X.S., Jiang, S.Y., Hu, J., Li, Z. (2007). Geochronology and geochemistry of the Yaokeng alkaline granitic pluton in Zhejiang province: Petrogenetic and tectonic implications. Acta Petrologica Sinica, 23, 1431-1440.

Yang, J.B., Zhao, Z.D., Hou, Q.Y., Niu, Y.L., Mo, X.X., Sheng, D., Wang, L.L. (2018). Petrogenesis of Cretaceous (133–84Ma) intermediate dykes and host granites in southeastern China: Implications for lithospheric extension, continental crustal growth, and geodynamics of Palaeo-Pacific subduction. Lithos, 296-299, 195-211.

Zhao, J.H., Hu, R.Z., Zhou, M.F., Liu, S. (2007). Elemental and Sr-Nd-Pb isotopic geochemistry of Mesozoic mafic intrusions in southern Fujian Province, SE China: implications for lithospheric mantle evolution. Geological Magazine, 144, 937-952.

Zhao, J.L., Qiu, J.S., Liu, L., Wang, R.Q. (2015). Geochronological, geochemical and Nd-Hf isotopic constraints on the petrogenesis of Late Cretaceous A-type granites from the southeastern coast of Fujian Province, South China. Journal of Asian Earth Sciences, 105, 338-359.

Zhao, J.L., Qiu, J.S., Liu, L., Wang. R.Q. (2016). The Late Cretaceous I- and A-type granite association of southeast China: Implications for the origin and evolution of post-collisional extensional magmatism. Lithos, 240, 16-33.

Zhou, X.M., Li, W.X. (2000). Origin of Late Mesozoic igneous rocks of southeastern China: implications for lithosphere subduction and underplating of mafic magma. Tectonophysics, 326, 269-287.

Zhou, X.M., Sun, T., Shen, W.Z., Shu, L.S., Niu, Y.L. (2006). Petrogenesis of Mesozoic granitoids

and volcanic rocks in South China: a response to tectonic evolution. Episodes, 29, 26-33.

Figure captions:

Figure 1 (a) Simplified geological map of major tectonic units in southeast continental China (after Chen, Lee, Lin, & Lu, 2006); (b) Simplified geological map of southeast continental China, showing the distribution of granitoids and our sample localities along the coast region (after Sun, 2006 and Niu, Shen, Shu, Sun, & Zhou, 2006). ZDSZ means Zhenghe-Dapu shear zone; CNSZ means Changle-nan'ao shear zone.

Figure 2 Photomicrographs of the granitoids, with (a) showing the contact of a finer-grained MME (FJS14-06MME) with the host granodiorite (FJS14-06host); (b)-(e) showing the mineralogy and textures of the granite samples (FJS14-06host, FJS14-17host, FJS14-01, FJS14-22); (f) showing the arfvedsonite in the Kuiqi alkali feldspar granite (FJS14-15) with the composition (electron-microprobe analysis) of SiO_2 = 51.65wt.%, Ti_2O = 0.12wt.%, Al_2O_3 = 0.26wt.%, Fe_2O_3 = 31.13wt.%, MnO_2 = 0.28wt.%, MgO = 0.00wt.%, CaO = 0.11wt.%, Na_2O = 12.53wt.%, and K_2O = 0.00wt.%. Qz-quartz, Amp-amphible, Mic-muscovite, Pl-plagioclase, Ap-apatite, Zrn-zircon, Kfs-K-feldspar, Bt-biotite and Arf-Arfvedsonite.

Figure 3 Cathodoluminescence (CL) images of zircon grains with LA-ICP-MS U-Pb dating spots as indicated and the Concordia diagrams for samples FJS14-01 (a, d), FJS14-08 (b, e) and FJS14-13 (c, f).

Figure 4 SiO_2/MgO variation diagrams of (a) TiO_2, (b) Al_2O_3, (c) $^{T}Fe_2O_3$, (d) CaO, (e) Na_2O, (f) P_2O_5 (g) K_2O, (h) A/NK Molar and (i) A/CNK Molar for our studied samples. Because

MgO is positively and SiO_2 is inversely related to the liquidus temperature, using the combined parameter of SiO_2/MgO can magnify and effectively illustrate the effect of varying extent of magma evolution on bulk-rock major and trace elements. The literature data are given in Appendix 7.

Figure 5 SiO_2/MgO variation diagrams of (a) Ba, (b) Eu/Eu*, (c) Nb, and (d) Rb/Sr. Sample symbols are the same as in Figure 4. The literature data are given in Appendix 8.

Figure 6 Photomicrographs showing small compositional variation (in terms of the An value defined as Ca/(Ca+Na); electron probe analysis) of selected plagioclase crystals in representative samples as indicated (Samples FJS14-06MME, FJS14-06host, FJS14-17MME, and FJS14-17host, respectively in panels a-d, respectively).

Figure 7 Sr-Nd-Hf isotope data. (a) $^{87}Sr/^{86}Sr_{(i)}$ vs. $\varepsilon Nd_{(t)}$; (b) $\varepsilon Nd_{(t)}$ vs. $\varepsilon Hf_{(t)}$; (c) and (d) Age vs. $\varepsilon Nd_{(t)}$ and $\varepsilon Hf_{(t)}$, respectively; (e) and (f) correlation of $\varepsilon Hf_{(t)}$ and $\varepsilon Nd_{(t)}$ as a function of latitude; and (g) Rb-Sr isochron of our samples. The data used to calculate the $^{87}Sr/^{86}Sr_{(i)}$, $\varepsilon Hf_{(t)}$, $\varepsilon Nd_{(t)}$ and the reference line of the depleted-mantle (DM) are given in Appendix 6. Binary isotope mixing calculations of (b) used the DM data from Salters and Stracke (2004) and the lower continental crust data from Rudnick and Gao (2003) and Shen et al. (1993). The data of line 1 and line 2 in (c) are from Shen et al. (1993). Sample symbols are the same as in Figure 4. The literature data are given in Appendix 9.

Figure 8 Granitoid classification diagrams of Whalen et al. (1987). (a) (1000*Ga/Al) vs. $(K_2O+Na_2O)/CaO$. (b) (Zr+Nb+Ce+Y) vs. $(K_2O+Na_2O)/CaO$. FG-fractionated felsic granites; OGT-unfractionated M-, I- and S-type granites. Sample symbols are the same as in Figure 4.

Figure 9 (a) $^{T}Fe_2O_3$ vs. SiO_2/MgO (wt. % on anhydrous basis). The pink line represents rhyolite-MELTS fractional crystallization modelling by assuming the most primitive Group 1 sample (FJS14-06host) as the parental granitoid liquid composition with water content of 6 wt. % at 3 kbar. The arrow indicates that the residual melt fraction decreases as temperature falls as a function of the increasing percentage (%) of crystallization. (b) Ba vs. Sr covariation, indicating that the sample compositional variation is largely caused by alkali-feldspar fractionation. The trend lines of fractional crystallization of minerals (Pl-plagioclase, Ap-apatite, Zrn-zircon, Kfs-K-feldspar and Bt-biotite) were calculated using the data from https://earthref.org/GERM/. Sample symbols are the same as in Figure 4.

Figure 10 (a) Conceptual model of the Cretaceous magmatism in a NW-SE cross section, which is roughly perpendicular to the coastal line and is interpreted to be consistent with the paleo-Pacific plate subduction (Niu et al., 2015). (b) Conceptual model of the SW-NE direction Cretaceous magmatism along the southeast coastline of continental China.

Table caption:

Table 1 Petrography of granitoid samples from southeast cost of continental China (N=16).

Appendices:

Appendix 1 Zircon U-Pb dating of the granitoids along the southeast coast of continental China.

Appendix 2 Geochronological data for the granitoids along the southeast coast of continental China.

Appendix 3 Whole-rock major elements compositions of the granitoids along the southeast coast of continental China.

Appendix 4 Whole-rock trace elements compositions of the granitoids along the southeast coast of continental China.

Appendix 5 Microprobe analysis of representative plagioclase of the granitoids along the southeast coast of continental China.

Appendix 6 Whole rock Sr-Nd-Hf isotopic composition for the granitoids along the southeast coast of continental China.

Appendix 7 Whole-rock major elements composition data from literature.

Appendix 8 Whole-rock trace elements composition data from literature.

Appendix 9 Whole rock Sr-Nd-Hf isotopic composition data from literature.

Appendix Figure Spider diagram of trace elements (a) Group 1; (b) Group 2; (c) Group 3.

Fig. 1

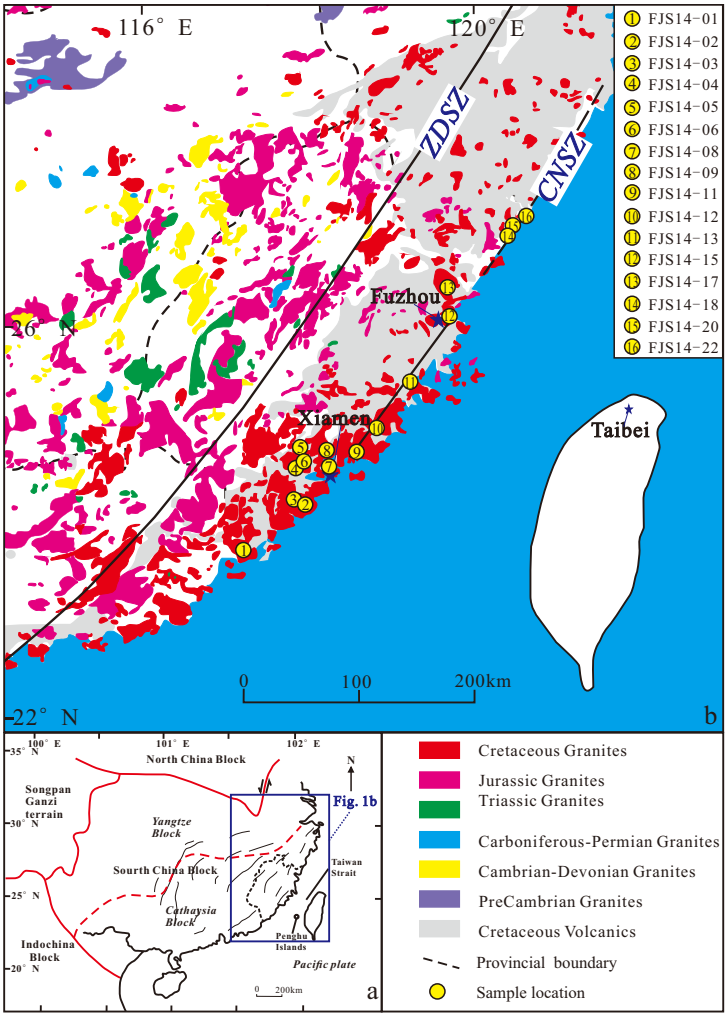
116° E
120° E
26° N
22° N
ZDSZ
CNSZ
Fuzhou
Xiamen
Taibei
0
100
200km
b
FJS14-01
FJS14-02
FJS14-03
FJS14-04
FJS14-05
FJS14-06
FJS14-08
FJS14-09
FJS14-11
FJS14-12
FJS14-13
FJS14-15
FJS14-17
FJS14-18
FJS14-20
FJS14-22
100° E
101° E
102° E
35° N
30° N
25° N
20° N
North China Block
Songpan Ganzi terrain
Yangtze Block
Sourth China Block
Cathaysia Block
Indochina Block
Taiwan Strait
Penghu Islands
Pacific plate
Fig. 1b
N
0 200km
a
Cretaceous Granites
Jurassic Granites
Triassic Granites
Carboniferous-Permian Granites
Cambrian-Devonian Granites
PreCambrian Granites
Cretaceous Volcanics
Provincial boundary
Sample location

Fig. 2

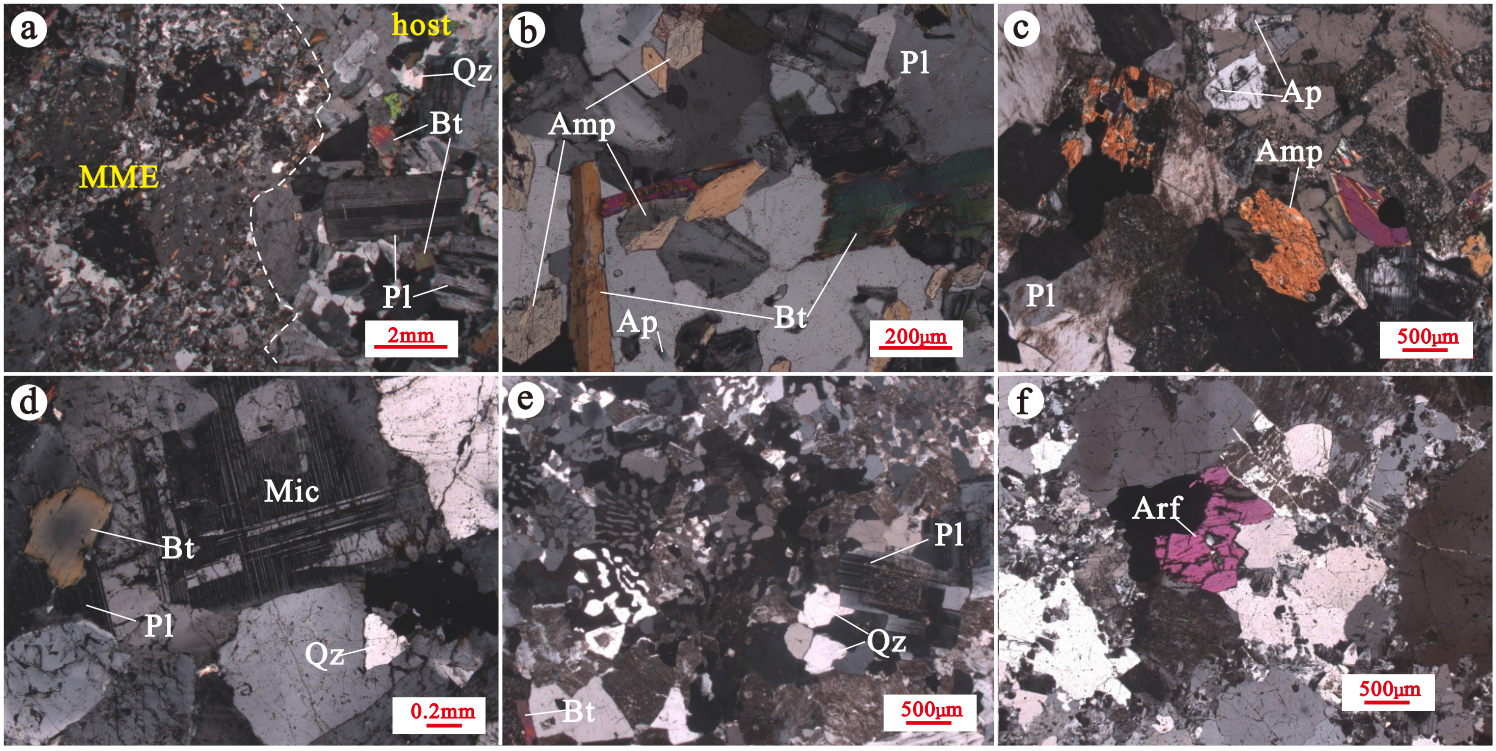
a
host
Qz
Bt
MME
Pl
2mm
b
Pl
Amp
Ap
Bt
200μm
c
Ap
Amp
Pl
500μm
d
Mic
Bt
Pl
Qz
0.2mm
e
Pl
Qz
Bt
500μm
f
Arf
500μm

Fig. 3

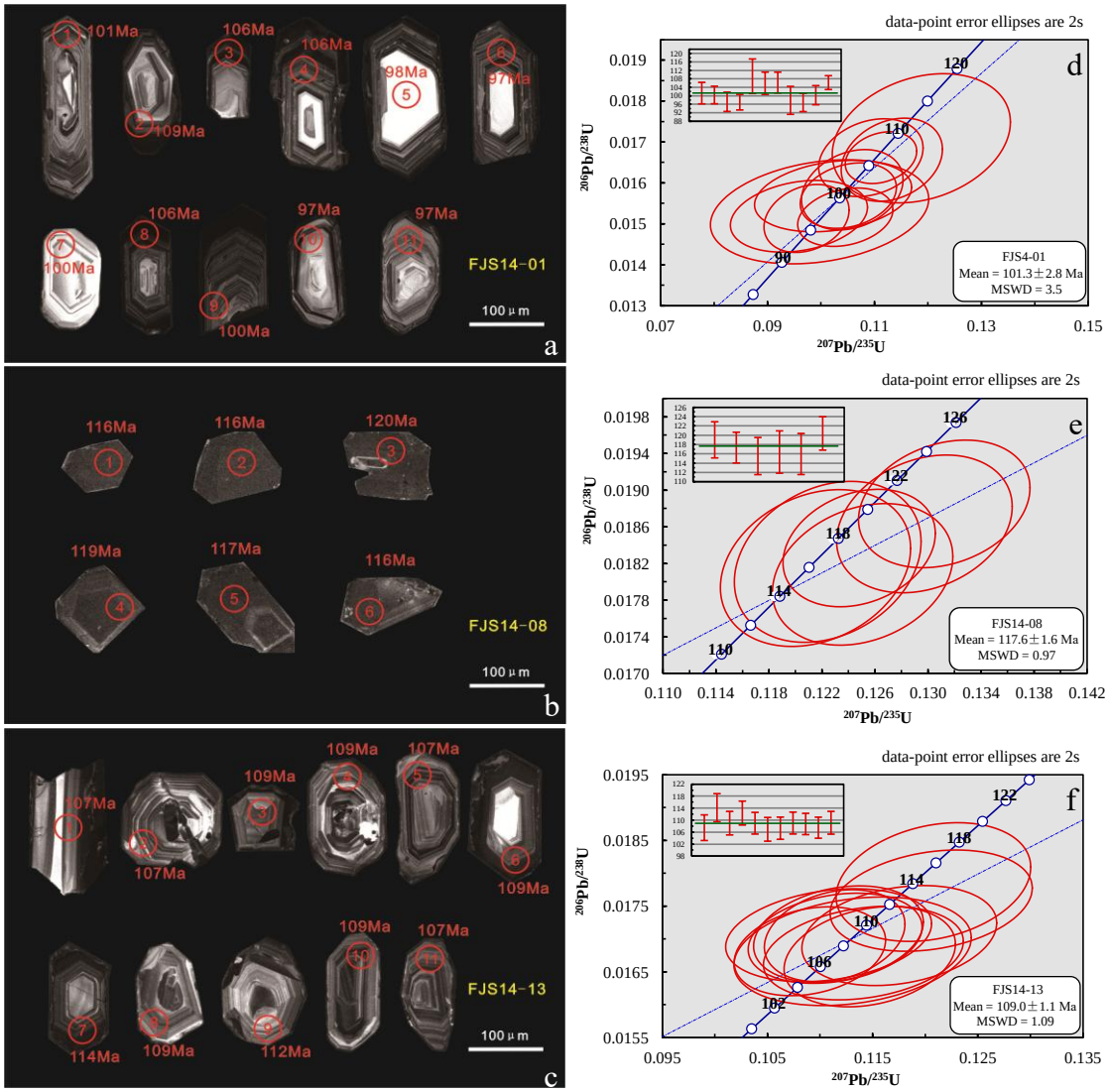
101Ma
106Ma
106Ma
98Ma
97Ma
109Ma
106Ma
97Ma
97Ma
100Ma
100Ma
FJS14-01
100 μm
a
116Ma
116Ma
120Ma
119Ma
117Ma
116Ma
FJS14-08
100 μm
b
109Ma
107Ma
109Ma
107Ma
107Ma
109Ma
109Ma
107Ma
114Ma
109Ma
112Ma
FJS14-13
100 μm
c
data-point error ellipses are 2s
d
FJS4-01
Mean = 101.3±2.8 Ma
MSWD = 3.5
206Pb/238U
207Pb/235U
data-point error ellipses are 2s
e
FJS14-08
Mean = 117.6±1.6 Ma
MSWD = 0.97
206Pb/238U
207Pb/235U
data-point error ellipses are 2s
f
FJS14-13
Mean = 109.0±1.1 Ma
MSWD = 1.09
206Pb/238U
207Pb/235U

Fig. 4

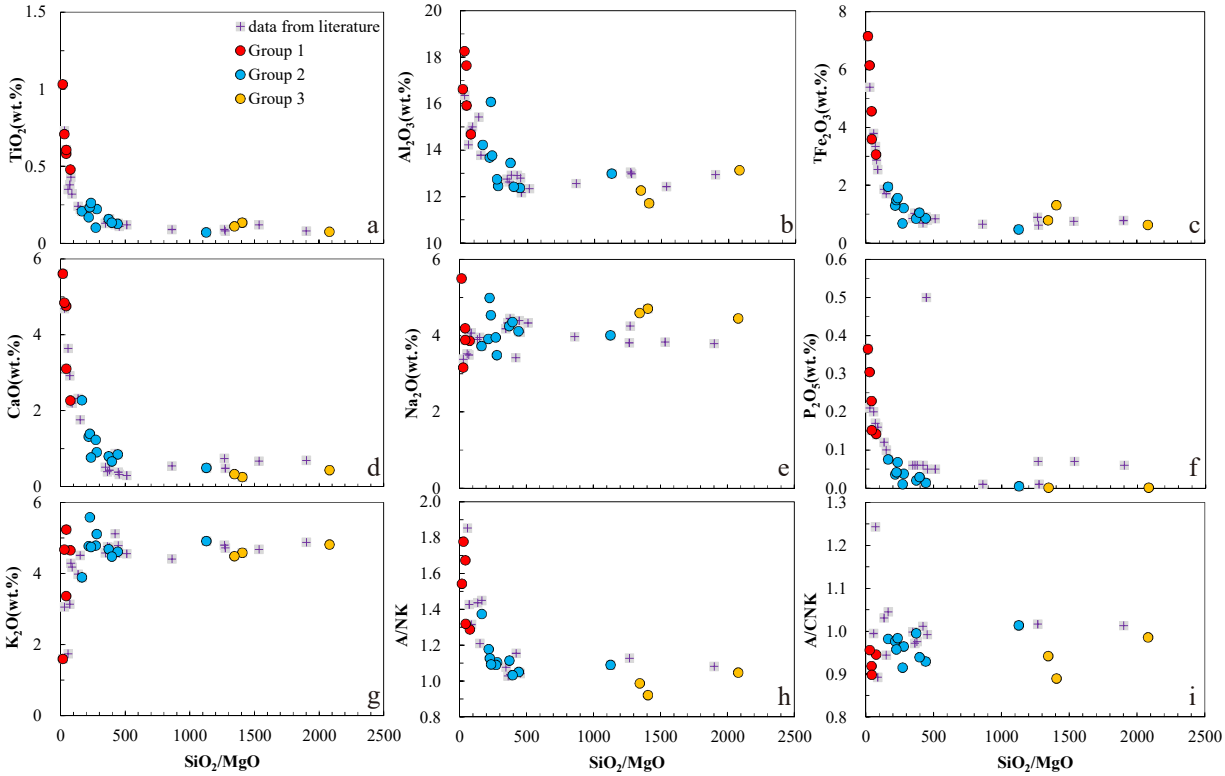
data from literature
Group 1
Group 2
Group 3
TiO2(wt.%)
Al2O3(wt.%)
TFe2O3(wt.%)
CaO(wt.%)
Na2O(wt.%)
P2O5(wt.%)
K2O(wt.%)
A/NK
A/CNK
SiO2/MgO
SiO2/MgO
SiO2/MgO
a
b
c
d
e
f
g
h
i

Fig. 5

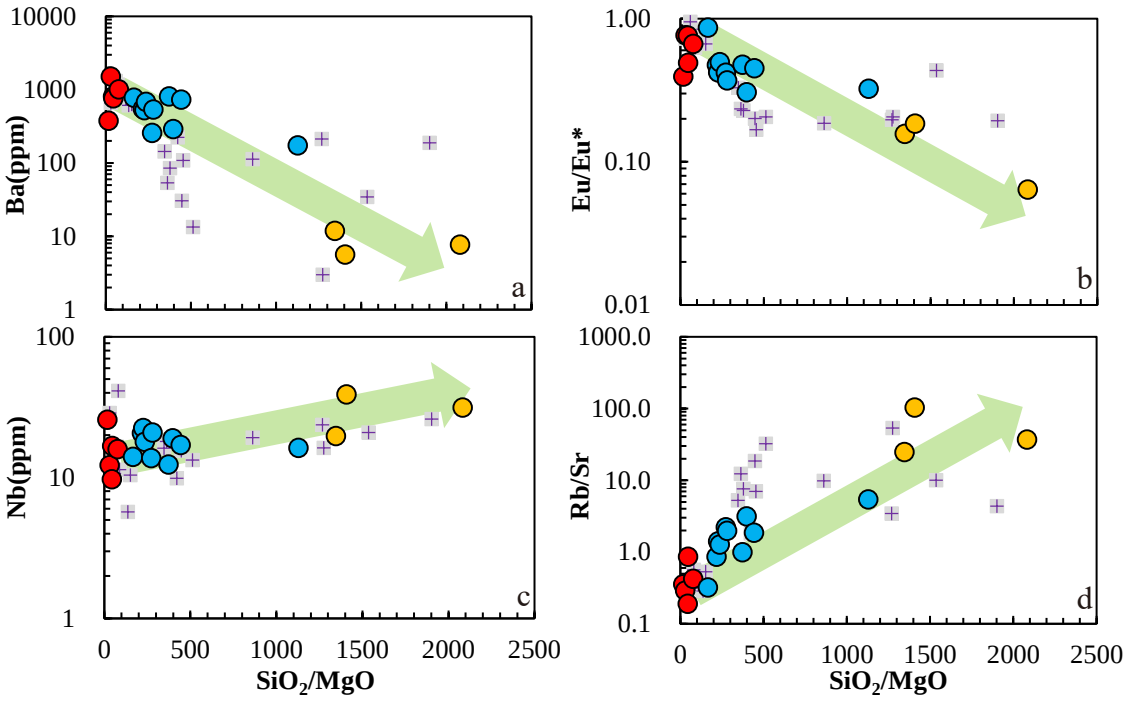
10000
1000
100
10
1
Ba(ppm)
a
1.00
0.10
0.01
Eu/Eu*
b
100
10
1
Nb(ppm)
c
1000.0
100.0
10.0
1.0
0.1
Rb/Sr
d
0
500
1000
1500
2000
2500
SiO2/MgO

Fig. 6

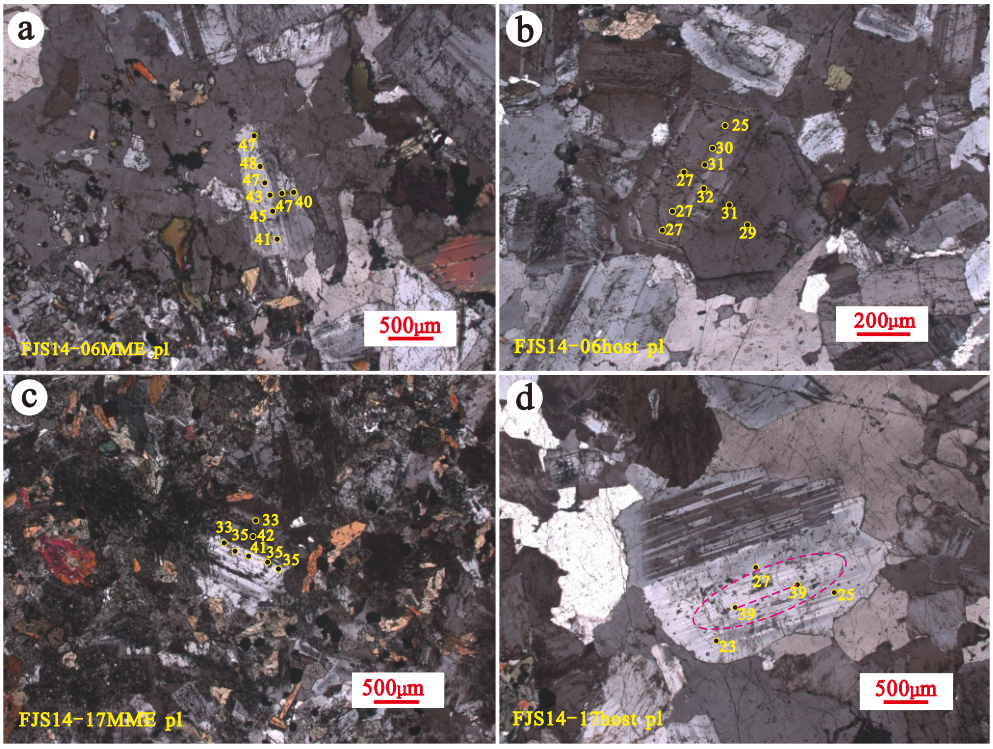
a
47
48
47
43
45
47
40
41
500μm
FJS14-06MME_pl
b
25
30
31
27
32
27
31
27
29
200μm
FJS14-06host_pl
c
33
33
35
42
41
35
35
500μm
FJS14-17MME_pl
d
27
32
25
29
23
500μm
FJS14-17host_pl

Fig. 7

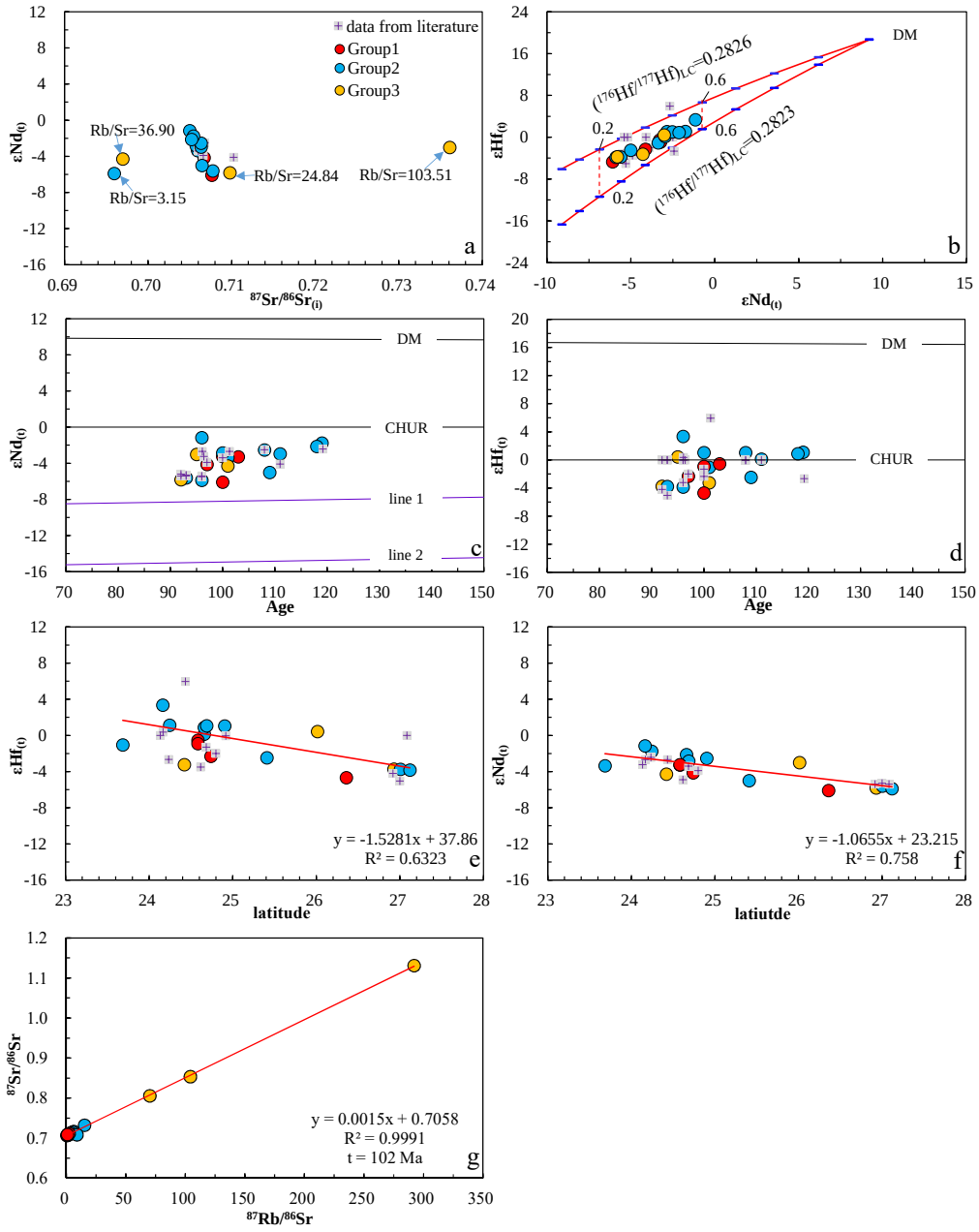
data from literature
Group1
Group2
Group3
Rb/Sr=36.90
Rb/Sr=3.15
Rb/Sr=24.84
Rb/Sr=103.51
a
εNd(t)
87Sr/86Sr(i)
DM
(176Hf/177Hf)LC=0.2826
(176Hf/177Hf)LC=0.2823
0.2
0.6
b
εHf(t)
CHUR
line 1
line 2
c
Age
d
y = -1.5281x + 37.86
R² = 0.6323
e
latitude
y = -1.0655x + 23.215
R² = 0.758
f
latiutde
y = 0.0015x + 0.7058
R² = 0.9991
t = 102 Ma
g
87Sr/86Sr
87Rb/86Sr

Fig. 8

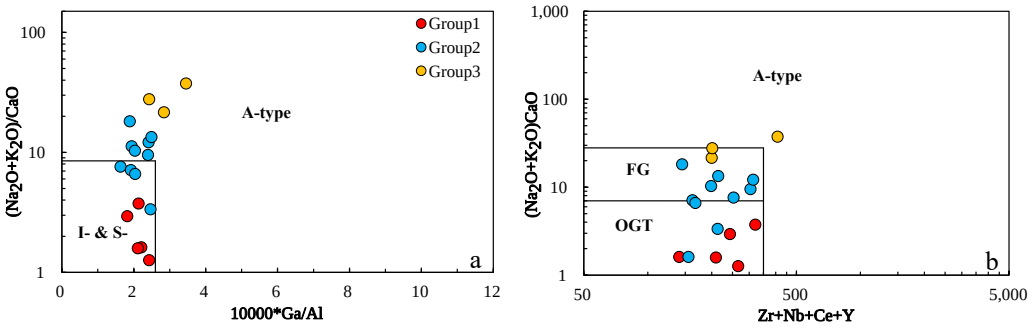
Group1
Group2
Group3
A-type
I- & S-
a
(Na2O+K2O)/CaO
10000*Ga/Al
100
10
1
0
2
4
6
8
10
12
A-type
FG
OGT
b
1,000
100
10
1
50
500
5,000
Zr+Nb+Ce+Y

Fig. 9

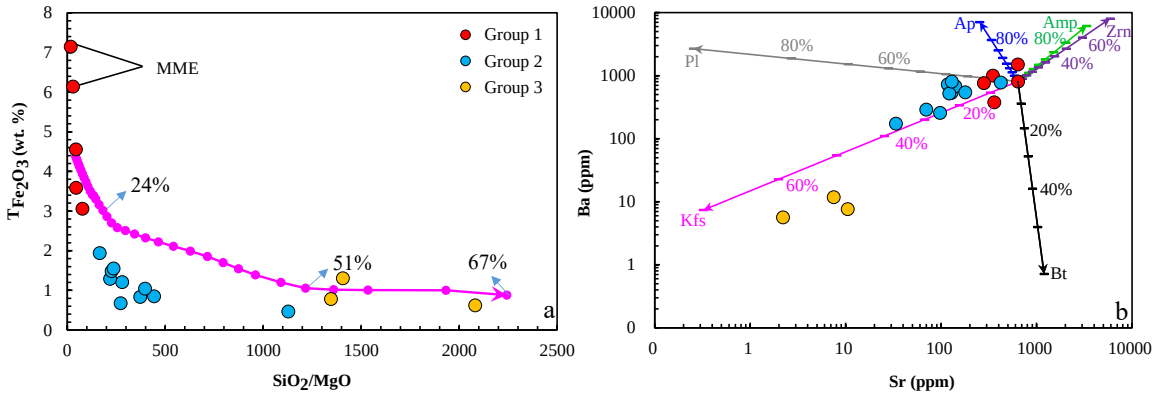
Group 1
Group 2
Group 3
MME
24%
51%
67%
a
$T_{Fe_2O_3}$ (wt. %)
SiO_2/MgO
Ap
Amp
Zrn
Pl
80%
60%
40%
20%
Kfs
Bt
b
Ba (ppm)
Sr (ppm)

Fig. 10

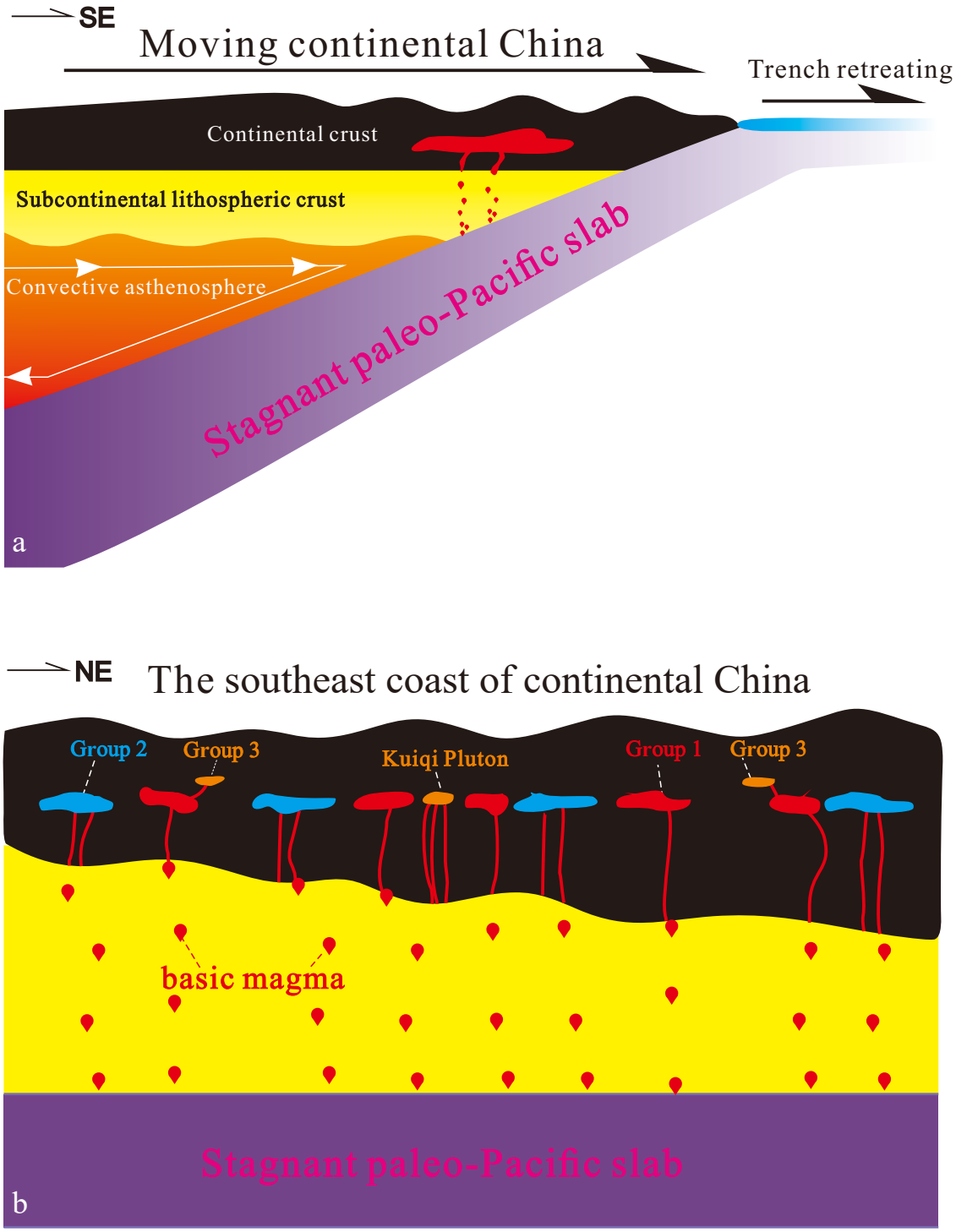
SE
Moving continental China
Trench retreating
Continental crust
Subcontinental lithospheric crust
Convective asthenosphere
Stagnant paleo-Pacific slab
a
NE
The southeast coast of continental China
Group 2
Group 3
Kuiqi Pluton
Group 1
Group 3
basic magma
Stagnant paleo-Pacific slab
b